IEEE Access
Multidisciplinary | Rapid Review | Open Access Journal

Received March 9, 2022, accepted April 4, 2022, date of publication April 7, 2022, date of current version April 14, 2022.

Digital Object Identifier 10.1109/ACCESS.2022.3165549

Optimized Design of Rotor Barriers in PM-Assisted Synchronous Reluctance Machines With Taguchi Method

MARYAM NASEH[1], SAEED HASANZADEH[1], SEYED MOHAMMAD DEHGHAN[1], HOSSEIN REZAEI[2], AND AMEENA SAAD AL-SUMAITI[3], (Senior Member, IEEE)

[1]Department of Electrical and Computer Engineering, Qom University of Technology, Qom 151937195, Iran
[2]Department of Electrical and Computer Engineering, Babol Noshirvani University of Technology, Babol 47148-71167, Iran
[3]Advanced Power and Energy Center, Khalifa University of Science and Technology, Abu Dhabi, United Arab Emirates

Corresponding author: Saeed Hasanzadeh (hasanzadeh@qut.ac.ir)

ABSTRACT In recent years, PM-assisted synchronous reluctance machines simplicity, robustness, efficiency, and temperature capacity (SynRMs) make them a viable alternative in various applications. The poor power factor (PF) and high torque ripple are the main challenges of SynRMs, which necessitate robust optimization improving the mentioned demerits. However, the optimization algorithms usually rely on complex analytical models; in this paper, in order to optimize, the design of experiments with the Taguchi method has been used. Taguchi is a simple and effective optimization method and requires a small number of experiments and experience. Also, to select the best combination in multi-objective optimization, the TOPSIS method has been utilized to prioritize the optimal solutions. The proposed method is evaluated by finite element analysis (FEA).

INDEX TERMS Permanent magnet (PM)-assisted synchronous reluctance machine (SynRM), multi-objective optimization, Taguchi method, finite element analysis (FEA), torque ripple.

I. INTRODUCTION

The absence of winding and magnet on the rotor of SynRMs leads to simplicity, robustness, low maintenance, lower rotor losses, better thermal management, and efficiency with respect to permanent magnet synchronous and induction machines (IM). Other advantages of SynRMs are less torque ripple, vibration, and noise compared to the switch reluctance machines (SRM), the high dynamic response, and wide-speed range [1]–[3]. However, the challenges of poor power factor and high torque ripple have limited the widespread development of SynRMs in industrial applications [1], [4]. Adding some permanent magnets to the SynRMs rotor core (PM-assisted SynRMs) can be considered as a solution attenuating disadvantages [5]. Increasing the power factor draws less stator input current. This leads to a decrease in the total loss and improves efficiency [2]. Although the share of reluctance torque is greater than the torque produced by PMs [1], [6], the magnet type strongly affects the average torque produced and the performance of the machine [7]. Strong and rare-earth PMs like NdFeB and SmCo offer good performance. However, they are not recommended in some applications due to their high cost [8]. On the other side, the PM-assisted SynRM with non-rare-earth PMs can be considered an alternative for PM machines that use fewer PMs [7]–[11]. Non-rare-earth PMs such as ferrite is suggested as financial and effective magnet suitable for light electric vehicle applications. Improving the performance of SynRM and owning their advantages gets significant attention in electric vehicles and traction applications, etc. [9], [12].

The shape and number of flux barriers are other factors that considerably impact achieving a higher saliency ratio and improving torque. In [13], the influence of rotor structure on the performance of PM-assisted SynRM, the number of poles, and the shape of the flux barrier to achieve high torque and high power have been investigated. The shape and number of flux barriers are usually determined using optimization algorithms to increase the power factor and average torque. In [14], the torque ripple and average torque are optimized via

The associate editor coordinating the review of this manuscript and approving it for publication was Bijoy Chand Chatterjee.

a stochastic optimization algorithm with the design variables of flux barrier angles and stator slot opening dimensions. In [12], using the Differential Evolution (DE) algorithm, the minimization of iron and copper losses is also considered by optimizing the main stator dimensions, insulation ratio, and flux barrier angles. Another DE algorithm is utilized to optimize the rotor geometry with the objectives of torque, loss, back-emf, THD, and material cost [15]. Later in [16], the effect of PM and flux barriers dimensions on the torque ripple of PM-assisted SynRMs has been investigated based on sensitivity and finite element analysis. The use of a nonlinear analysis model of SynRMs to extract both average torque and torque harmonics as a function of rotor geometry is proposed in [17]. However, the most reported articles that deal with the optimized design of SynRM usually necessitate accurate analytical models for computing the objective function in an iterative algorithm. Also, the analytical model-free methods such as sensitivity analysis rely on many finite element results, which is time-consuming with high computational effort.

In this paper, the Design of Experiments (DOE) with Taguchi method for optimizing the torque, torque ripple, and total harmonic distortion (THD) is suggested, which does not require complex and analytical models. Using Taguchi method, the impact of parameters is evaluated with a minimum number of finite element results. The Technique for Order of Preference by Similarity to Ideal Solution (TOPSIS) offers the best decision faster than other Decision-Making Algorithms (DMA) [18]. In this study, the TOPSIS algorithm is chosen as a simple and effective method to prioritize optimal solutions.

The organization of this paper is as follows. In Section II, first, the characteristics of PM-assisted SynRM will be expressed. After that, the multi-objective optimization method, including the DOE with Taguchi method, DMA with TOPSIS, will be discussed. Finally, in Section III, the performance of optimized PM-assisted SynRM is analyzed according to finite element simulations.

II. MULTI-OBJECTIVE OPTIMIZATION

The optimization objective is to find the best value from a group of possible values to attenuate the challenges. In the multi-objective optimization with Taguchi method, an engineering and optimization method is required to judge the best combination of parameters. In order to optimize the machine proposed in [1], DOE with Taguchi method are incorporated, and to select the best combination of experiments, TOPSIS has been used.

A. THE INITIAL DESIGN OF PM-ASSISTED SYNRM

The original geometric design of three-phase PM-assisted SynRM is chosen according to [1] and listed in Table 1. The rotor of this machine is a TLA type consisting of four flux barriers at each pole with the 19.6 mm length of low-cost AlNiCo9 PMs placed between the flux barriers. Although in the PM-assisted SynRM, the PMs are often established inside flux barriers, in this topology, the PMs are located in the rotor iron part to fully utilize PM flux as depicted in Fig. 1.

TABLE 1. Original design of PM-assisted SynRM characteristics [1].

Parameter	value
Winding type	Distributed/ Single layer
Number of windings turns per slot	25
Coil pitch	9 slots
Rated current	20 A
Stack length	200 mm
Air gap	0.4 mm
Rotor Outer diameter	134.2 mm
Stator Outer diameter	204.8 mm
Number of poles/ stator slots	4/36
Stator and rotor core material	M15G29, Mass density =7650 (Kg/m^3)
Permanent magnet material	AlNiCo9, B_r=1.08 T, H_c=120 KA/m, Mass density =7000 (Kg/m^3)

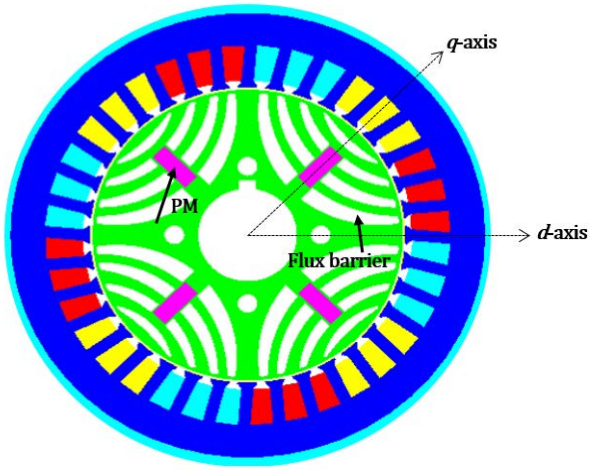

FIGURE 1. The initial design of PM-assisted SynRM.

B. DESIGN OF EXPERIMENTS WITH TAGUCHI METHOD

The ability to observe and identify the output changes through conscious changes in the process input variables is one of the purposes of designing experiments. At the first step in Taguchi method, the parameters are selected, and their levels are estimated. After that, the DOE is performed, and at the last step, the optimization results are reviewed [19].

In this study, the optimization variables are estimated first. Therefore, five design variables with five levels are considered as follows:

1- BR01, the thickness of the first flux barrier end (A), 2- BR00, the thickness of the second, third, and fourth flux barrier end (B), 3- BR3, the thickness of the third flux barrier (C), 4- BR2, the thickness of the fourth flux barrier (D) and 5- BR4 thickness of the second flux barrier (E). The design variables are shown in Fig. 2. The average torque, torque ripple, efficiency, THD of phase voltage and PF are considered as multi-objective optimization goals to achieve the

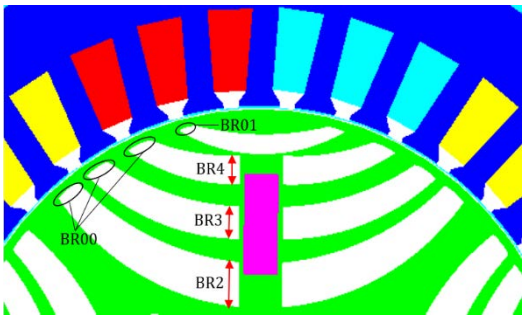

FIGURE 2. Design variables of the proposed machine.

highest average torque value, PF and efficiency, minimum torque ripple, and THD phase voltage. In this paper, our main emphasis is on improving the torque characteristics, while maintaining the other performance indexes such as efficiency, power factor and THD by neglecting their small changes. The initial information of design variables and their levels are listed in Table 2. After preparing the initial data, DOE is carried out.

TABLE 2. Design variables and their levels.

LEVELS	PARAMETER				
	A	B	C	D	E
Level 1	0.5	1	2.4	5	2.5
Level 2	1.5	2	3.4	6	3.5
Level 3	2.5	3	4.4	7	4.5
Level 4	3.5	4	5.4	8	5.5
Level 5	4.5	5	6.4	9	6.5

The orthogonal arrays are shown in Table 3. An orthogonal array is a matrix provided with the Taguchi method whose columns represent the design variables, and its rows indicate the level of factors in each experiment [19]. The results of various experiments are shown in Table 4.

After implementing the experiments, Analysis of Mean (ANOM) is used for statistical analysis of results, and the average of the objective functions in each level of design variable is calculated [18]. The ANOM results of the experiments are shown in Fig. 3.

A statistical method called Analysis of Variance (ANOVA) is used to find the relative importance of the parameters on each output. The variance of each design variable for each objective function is calculated.

$$v_x = \sum_{i=1}^{5} (f_{mxi} - f_m)^2 \tag{1}$$

where f_{mxi}, f_m, and v_x are the average of objective functions in the ith level of the design variable x, the overall mean of objective functions, and variance of the design variable x for an objective function, respectively. Also, the ratio of the effect of each design variable on the objective functions can

TABLE 3. Orthogonal arrays.

exam	Levels of design variables				
	A	B	C	D	E
1	1	1	1	1	1
2	1	2	2	2	2
3	1	3	3	3	3
4	1	4	4	4	4
5	1	5	5	5	5
6	2	1	2	3	4
7	2	2	3	4	5
8	2	3	4	5	1
9	2	4	5	1	2
10	2	5	1	2	3
11	3	1	3	5	2
12	3	2	4	1	3
13	3	3	5	2	4
14	3	4	1	3	5
15	3	5	2	4	1
16	4	1	4	2	5
17	4	2	5	3	1
18	4	3	1	4	2
19	4	4	2	5	3
20	4	5	3	1	4
21	5	1	5	4	3
22	5	2	1	5	4
23	5	3	2	1	5
24	5	4	3	2	1
25	5	5	4	3	2

TABLE 4. Results of experiments.

exam	T_ave	Ripple (%)	Efficiency (%)	THD (%)	PF
1	48.75	19.455	74.349	11.694	0.774
2	57.67	14.574	78.260	10.121	0.739
3	64.12	12.817	80.451	8.931	0.711
4	67.36	12.556	81.379	8.413	0.693
5	68.51	10.366	81.698	9.432	0.680
6	57.61	14.901	78.238	10.341	0.740
7	63.39	17.306	80.213	9.146	0.714
8	66.04	15.479	81.026	8.444	0.703
9	64.20	11.470	80.428	10.203	0.709
10	62.78	11.016	80.005	10.371	0.713
11	59.90	16.183	79.060	9.174	0.734
12	60.11	18.498	79.074	11.312	0.729
13	64.99	12.354	80.694	9.519	0.706
14	62.78	11.016	80.220	10.379	0.713
15	65.43	13.608	80.821	9.218	0.701
16	59.00	14.641	78.701	10.84	0.734
17	63.37	10.032	80.171	8.995	0.715
18	63.65	11.698	80.326	9.315	0.713
19	67.10	9.713	81.277	8.671	0.696
20	64.94	11.771	80.620	11.178	0.703
21	61.45	15.799	79.588	9.182	0.723
22	63.44	11.707	80.220	9.503	0.715
23	62.09	18.754	79.791	11.660	0.719
24	63.87	9.206	80.352	9.607	0.711
25	67.40	13.466	81.363	9.252	0.691

be calculated as

$$I_x = \frac{v_x}{\sum_{s=1}^{5} v_s} \tag{2}$$

in which I_x and s are the ratios of the design variable x on the objective function and the number of design variables, respectively. The results of the ratio of the effect of each parameter on the objective functions are shown in Table 5.

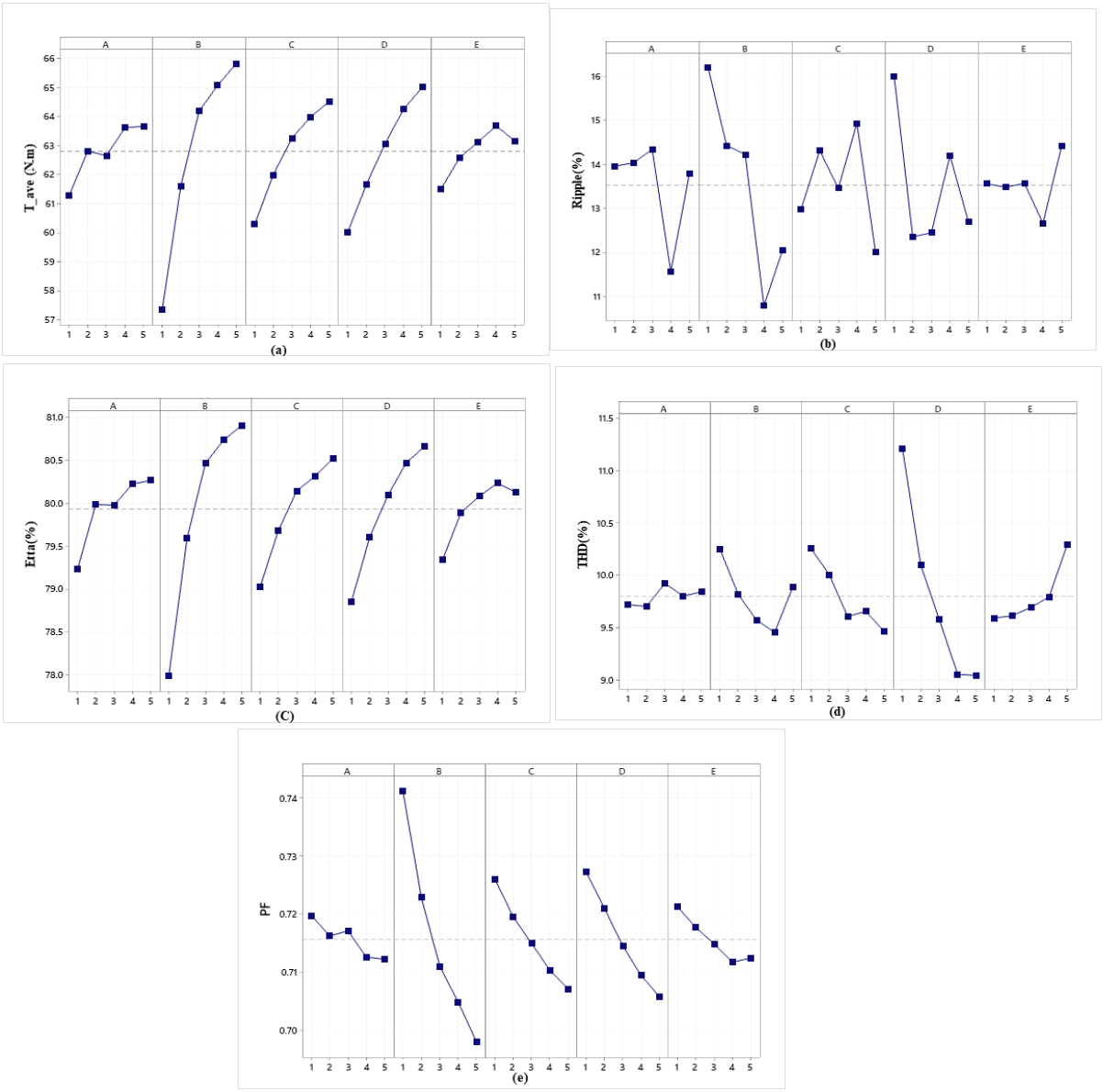

FIGURE 3. Analysis of mean (a) average torque, (b) torque ripple, (c) efficiency, (d) THD, (e) PF.

TABLE 5. The ratio of the effect of each parameter on the objective functions.

Objective Function	Design variables				
	A	B	C	D	E
Average-Torque	3.88%	57.51%	13.46%	19.04%	2.69%
Torque Ripple (%)	8.39%	41.42%	8.95%	20.40%	0%
Efficiency (%)	4.86%	53.24%	11.76%	18.39%	2.98%
THD (%)	0%	7.36%	8.17%	72.12%	6.31%
Power Factor (%)	2.06%	64.80%	12.29%	16.58%	3.27%

Table 6 shows the optimal combination of design variables for each objective function. Results show that the fourth level of B parameter is the optimal level for torque ripple and THD, while the fifth level of B parameter leads to the maximum average torque and efficiency. Furthermore, the fifth level of D parameter has the highest average torque and efficiency and the lowest THD, and the torque ripple value is low at this level. Therefore, the fifth level of D parameter is due to the high effect (72.12%) on THD compared to other objective functions, and the optimality of average torque and efficiency at this level has been selected as the optimal level. In the fourth level of E parameter, the maximum amount of torque and efficiency and minimum torque ripple is observed. The fourth level has been selected as the best level with the lowest torque ripple in the A parameter. The fifth level of C parameter also has the maximum torque and efficiency and the minimum torque ripple and THD.

TABLE 6. Optimal combination of design variables for each objective function.

objective functions	Design variables				
	A	B	C	D	E
Average-Torque	5	5	5	5	4
Torque Ripple (%)	4	4	5	2	4
Efficiency (%)	5	5	5	5	4
THD (%)	2	4	5	5	1
PF	1	1	1	1	1

TABLE 7. The optimal possible combination of design variables.

	Design variables					objective functions				
	A	B	C	D	E	T-Ave	Ripple	η	THD	PF
Case1	4	5	5	5	4	68.3	9.97	81.6	9.74	0.682
Case2	4	5	3	5	4	67.7	10.75	81.4	9.32	0.688
Case3	4	4	5	5	4	68.69	15.5	81.7	9.69	0.685
Case4	4	4	3	5	4	67.8	11.03	81.4	8.74	0.692
Initial design	2	3	4	3	3	65.28	12.208	80.7	8.88	0.706

The optimal possible combination of design variables is listed in Table 7. In Case 1, the average torque and efficiency have increased compared to the initial design, 4.68%, and 1.013%, respectively, and the torque ripple has decreased 18.29%, but the THD has slightly (9.64%) increased, so Case 1 emphasizes the reduction of the torque ripple. In Case 2, the average torque increased by 3.82% compared to the initial design, and the torque ripple has decreased 11.88%, efficiency increased slightly 0.82%, but the THD has increased 4.98%. The average torque and efficiency improved in case 3 5.23% and 1.17%, respectively, but the torque ripple and THD increased, 27% and 9.14%, respectively. In case 4, the average torque rises 3.86%, efficiency increased slightly 0.815%, the torque ripple and THD decreased 9.64% and 1.52%, respectively, and this mode emphasizes the improvement of THD. There is a considerable improvement in the average torque and torque ripple in all cases, while other performance indices such as PF are constant estimates. Then, TOPSIS is used to find the optimal combination in the multi-objective optimization problem.

C. TOPSIS METHOD

The TOPSIS algorithm is a powerful multi-criteria compensation technique for prioritizing options by simulating the ideal answer. In this method, the selected option must have the shortest distance from the ideal response and the farthest distance from the most inefficient response [18]. The steps for choosing the optimal solution based on the TOPSIS method are as follows:

1) CREATE DECISION MATRICES FOR RANKING

D is a decision matrix whose first, second, and third columns are the average torque, ripple torque, and THD, respectively. Rows represent the possible optimal combination of design variables, named as cases 1 to 4.

$$D = \begin{bmatrix} 68.33 & 9.97 & 9.74 \\ 67.77 & 10.75 & 9.32 \\ 68.69 & 15.5 & 9.69 \\ 67.80 & 11.03 & 8.74 \end{bmatrix} \tag{3}$$

2) STANDARDIZE DATA AND FORM A STANDARD MATRIX

$$R_{ij} = \frac{X_{ij}}{\sum_{i=1}^{m} X_{ij}} \tag{4}$$

The matrix D is normalized by Equation (4). Where R_{ij}, X, and m represent the normalized matrix, the matrix element, and the number of cases, respectively.

3) DETERMINE THE WEIGHT OF EACH INDICATOR ($\sum_{i=1}^{n} w_i = 1$)

Then the objective functions are weighted. As a result, the weighted decision matrix is calculated as

$$V_{ij} = w_j \times R_{ij} \tag{5}$$

In this regard, more important indicators have a higher weight. V_{ij} and w_j represent the weighted decision matrix and weights, respectively.

4) DETERMINE THE HIGHEST PERFORMANCE OF EACH INDICATOR

The highest performance of each index is displayed with A^+ and the lowest performance of each index with A^-. Finding positive ideal solution (PIS) and negative ideal solution (NIS) is as follows:

$$\begin{aligned} A^+ &= \left\{V_1^+, V_2^+, \cdots V_m^+\right\} \\ V_j^+ &= \left\{\left(\max\left(V_{ij}\right) if\ j \in J\right); \left(\min\left(V_{ij}\right) if\ j \in J'\right)\right\} \\ A^- &= \left\{V_1^-, V_2^-, \cdots V_m^-\right\} \\ V_j^- &= \left\{\left(\min\left(V_{ij}\right) if\ j \in J\right); \left(\max\left(V_{ij}\right) if\ j \in J'\right)\right\} \end{aligned} \tag{6}$$

A^+, A^-, J, J, V_j^+, and V_j^- represent PIS, NIS, beneficial characteristics, non-beneficial characteristics, PIS, and NIS in a jth column, respectively. The average torque, efficiency, and PF are positive characteristics, while torque ripple and THD are negative.

5) FIND THE SEPARATION DISTANCE BETWEEN EACH OPTION TO PIS AND NIS

$$\begin{aligned} S_i^+ &= \sqrt{\sum_{j=1}^{n_0}\left(V_j^+ - V_{ij}\right)^2} \\ S_i^- &= \sqrt{\sum_{j=1}^{n_0}\left(V_j^- - V_{ij}\right)^2} \end{aligned} \tag{7}$$

The separation distance of each possible optimal combination from PIS and NIS is obtained from Equation (7). Where S_i^+ and S_i^- indicate the separation distance of ith possible optimum combination from PIS and NIS, and n_0 is the number of possible optimum combinations.

6) DETERMINE THE COEFFICIENT OF PROXIMITY TO EACH OF THE OPTIONS

In the last stage, the relative proximity of each possible optimal combination to the ideal solution to achieve the desired state is calculated.

$$C_i = \frac{S_i^-}{S_i^- + S_i^+} \tag{8}$$

This value fluctuates between $0 \leq \text{Ci} \leq 1$ and $\text{Ci} = 1$ and indicates the highest rank. $\text{Ci} = 0$ indicates the lowest rank. In this section, four choices with different weights are considered, and for all four cases, the value of Ci is calculated, and the results are listed in Table 8.

TABLE 8. The closest case to the ideal solution (C_I).

	weighting factors	Case1	Case2	Case3	Case4
select1	1/3; 1/3 1/3	0.99108	0.97071	0.00152	0.94691
select2	2/3; 1/6; 1/6	0.98917	0.95451	0.01421	0.93065
select3	1/6; 2/3; 1/6	0.99943	0.97344	$9.61E^{-05}$	0.94732
select4	1/6; 1/6; 2/3	0.87576	0.94589	0.01075	0.95537

In selection 1, the weighting factors of the average torque, torque ripple, and THD are considered equally. Dependent on the designer's priority, the weighting factor of the average torque maybe twice in selection 2. The same weighting factor can be applied to prioritize torque ripple and THD in the selections 3 and 4, respectively. According to Table 8, for all three selections (1, 2, and 3) with different weighting factors, Case 1 has a higher value of Ci and is selected as the optimal combination of design variables for the proposed motor.

III. OPTIMAL COMBINATION SIMULATION

In this section, the optimal model is simulated via finite element analysis and the outputs are examined as depicted in Fig. 4. The output torque in terms of rotor angle for the selected points is plotted in Fig. 5. As can be seen from Table 9, all selected points have higher average torque than the original design. In Case 1, as the first optimum design, the average torque increases to 68.33 N.m (4.68% change), and the torque ripple decreases to 9.97% (18.28% change), while there is a 1% improvement in efficiency. Moreover, THD and PF did not change considerably in the optimum points.

A. TORQUE RIPPLE MITIGATION

As indicated earlier, one of the main disadvantages of PM-assisted SynRM is its high torque ripple. A point with the minimum torque ripple is searched to further emphasize this issue using sensitivity analysis.

At the first step, the torque ripple is considered as a single-objective function, and among the 25 experiments proposed by Taguchi method, an experiment with levels BR01 = 5 (4.5 mm), BR00 = 4 (4 mm), BR3 = 3 (4.4 mm), BR2 = 2 (6 mm), BR4 = 1 (2.5 mm), with 9.2% torque ripple is

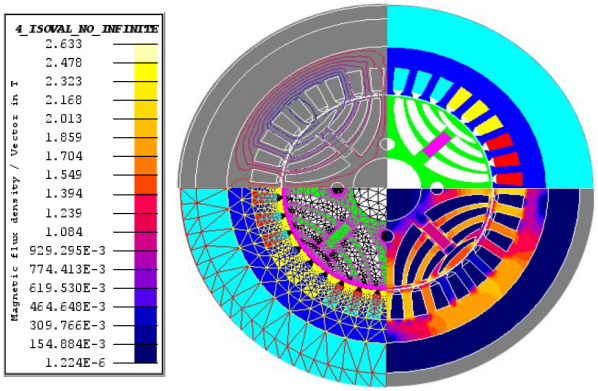

FIGURE 4. Simulation of the optimized model.

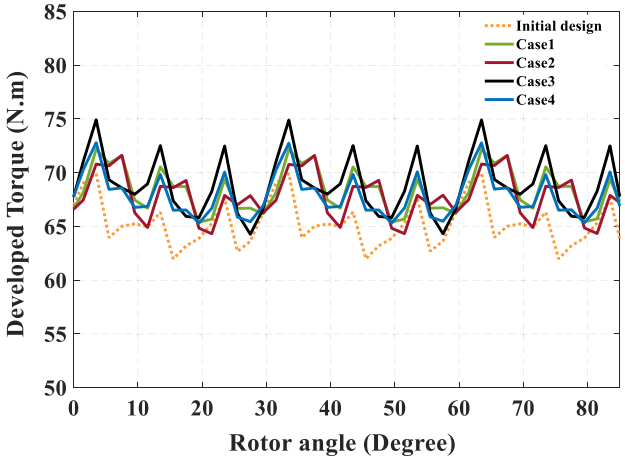

FIGURE 5. Comparison of average torque in various models.

TABLE 9. Comparison of different models.

	Average-Torque	Torque Ripple (%)	Efficiency (%)	THD (%)	PF
INITIAL DESIGN	65.28	12.208	80.7	8.88	0.706
CASE 1	68.3	9.97	81.6	9.74	0.682
CASE 2	67.7	10.75	81.4	9.32	0.688
CASE 3	68.69	15.5	81.7	9.69	0.685
CASE 4	67.8	11.03	81.4	8.74	0.692

TABLE 10. Torque ripple changes concerning BR01.

BR01	BR00	BR3	BR2	BR4	minimum torque ripple
4.3	4	4.4	6	2.5	9.25
4.4	4	4.4	6	2.5	9.15
4.5	4	4.4	6	2.5	9.21
4.6	4	4.4	6	2.5	9.17
4.7	4	4.4	6	2.5	9.07

selected, which has the lowest ripple rate among all scenarios. Since the optimization is performed on discrete points and there is a possibility of an optimal point in the vicinity of those discrete points, the sensitivity analysis is performed at this point in to achieve less torque ripple. At the next step,

TABLE 11. Torque ripple changes concerning BR2.

BR01	BR00	BR3	BR2	BR4	minimum torque ripple
4.7	4	4.4	5.8	2.5	9.68
4.7	4	4.4	5.9	2.5	9.37
4.7	4	4.4	6	2.5	9.07
4.7	4	4.4	6.1	2.5	8.86
4.7	4	4.4	6.2	2.5	8.66

TABLE 12. Torque ripple changes concerning BR4.

BR01	BR00	BR3	BR2	BR4	minimum torque ripple
4.7	4	4.4	6.2	2.3	8.63
4.7	4	4.4	6.2	2.4	8.65
4.7	4	4.4	6.2	2.5	8.66
4.7	4	4.4	6.2	2.6	8.7
4.7	4	4.4	6.2	2.7	8.72

TABLE 13. Torque ripple changes concerning BR3.

BR01	BR00	BR3	BR2	BR4	minimum torque ripple
4.7	4	4.2	6.2	2.3	8.7
4.7	4	4.3	6.2	2.3	8.64
4.7	4	4.4	6.2	2.3	8.62
4.7	4	4.5	6.2	2.3	8.6
4.7	4	4.6	6.2	2.3	8.58

TABLE 14. Torque ripple changes concerning BR00.

BR01	BR00	BR3	BR2	BR4	minimum torque ripple
4.7	3.8	4.6	6.2	2.3	8.6
4.7	3.9	4.6	6.2	2.3	8.56
4.7	4	4.6	6.2	2.3	8.58
4.7	4.1	4.6	6.2	2.3	8.6
4.7	4.2	4.6	6.2	2.3	8.62

TABLE 15. Comparison of optimal points specifications with the initial design.

						Initial design	1st Optimum Design (Case 1)	2nd Optimum Design (minimum torque ripple)
Barrier dimensions (mm)						(1.5, 3, 5.4, 7, 4.5)	(3.5, 5, 6.4, 9, 5.5)	(4.7, 3.9, 4.6, 6.2, 2.3)
BR01	BR00	BR3	BR2	BR4				
Average-Torque (N-m)						65.28	68.3 (+4.7%)	64.25 (-1.6%)
Torque Ripple (%)						12.208	9.97 (-18.3%)	8.56 (-29.9%)
Efficiency (%)						80.7	81.6 (+1.1%)	80.5 (-0.2%)
THD (%)						8.88	9.74 (+9.7%)	9.36 (+5.4%)
PF						0.706	0.682 (-3.4%)	0.709 (+0.4%)

a sensitivity analysis is performed around BR01 = 4.5 mm, and the width of 4.7 mm is selected with the minimum torque ripple, as shown in Table 10. As listed in Tables 11-14, the same sensitivity analysis is performed around BR2, BR4, BR3, and BR00 for achieving the lowest torque ripple.

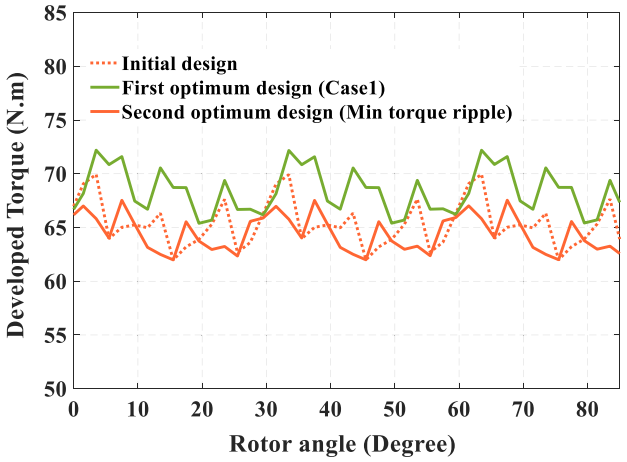

FIGURE 6. Comparison of torque in the initial design and first and second optimum design.

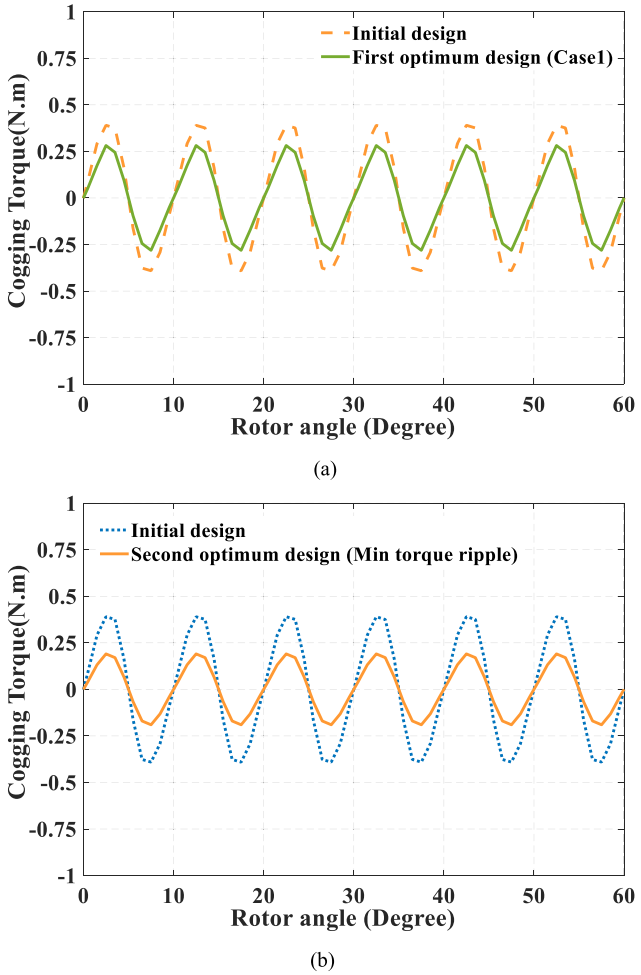

FIGURE 7. Comparison of cogging torque in the various designs (a) Initial design versus case 1 (b) Initial design versus minimum torque ripple.

The characteristics of the point with the minimum torque ripple are shown in Table 15. This point with minimum torque ripple is selected as the second optimum design.

The developed torque for the first and second optimum with respect to its initial designs are drawn in Fig. 6. As listed in TABLE 15, the torque ripple has decreased significantly (29.9% reduction) compared to the initial design. In comparison, the average torque has decreased slightly (1.6% reduction), THD increased slightly (5.4% change), and the efficiency and PF have not changed noticeably. Although the selected optimum point is achieved via a single-objective optimization of torque ripple, the torque ripple improves considerably without deteriorating other performance factors.

B. COGGING TORQUE

According to Fig. 7, in the first optimum design (case 1), the cogging torque decreases from 0.3903 to 0.2817 N.m (27.8% change) compared to the initial design. Besides that, the cogging torque at the second optimum design with minimum torque ripple has reached 0.1904 N.m, which has decreased (51.2%) compared to the initial design.

IV. CONCLUSION

In this paper, the optimization of PM-assisted SynRM is conducted by using the design of the experiment with Taguchi method. The five widths of the flux barrier are selected as design variables. With the main emphasis on improving the torque characteristics, the objective functions, including indices of average torque, torque ripple, and THD, are calculated via finite element analysis. The optimal model has been selected using TOPSIS method to achieve the best performance in multi-objective optimization. In the first optimum design, the average torque, torque ripple, and efficiency have improved with a 4.7% increase, 18.3% decrease, and 1.1% increase, respectively. However, the power factor does not change so much and is slightly worse.

Sensitivity analysis was performed to find the point with the lowest torque ripple as the second optimum design. At this design, the torque ripple decreased significantly compared to the initial design (29.9%), and the average torque decreased slightly (1.6%), whereas the power factor has not changed so much with a 0.4% improvement. The cogging torque has also reduced from 0.3903 to 0.2817 N.m and 0.1904 N.m in the first and second optimized models.

REFERENCES

[1] S. S. Maroufian and P. Pillay, "Design and analysis of a novel PM-assisted synchronous reluctance machine topology with AlNiCo magnets," *IEEE Trans. Ind. Appl.*, vol. 55, no. 5, pp. 4733–4742, Sep./Oct. 2019.

[2] H. Heidari, E. Andriushchenko, A. Rassolkin, A. Kallaste, T. Vaimann, and G. L. Demidova, "Comparison of synchronous reluctance machine and permanent magnet-assisted synchronous reluctance machine performance characteristics," in *Proc. 27th Int. Workshop Electr. Drives, MPEI Dept. Electr. Drives 90th Anniversary (IWED)*, Jan. 2020, pp. 1–5.

[3] Z. Zhang and L. Zhou, "Design and rotor geometry analysis of permanent magnet–assisted synchronous reluctance machines using ferrite magnet," *J. Electr. Eng.*, vol. 66, no. 6, pp. 311–316, Dec. 2015.

[4] C. Liu, K. Wang, S. Wang, Y. Wang, and J. Zhu, "Torque ripple reduction of synchronous reluctance machine by using asymmetrical barriers and hybrid magnetic core," *CES Trans. Electr. Mach. Syst.*, vol. 5, no. 1, pp. 13–20, Mar. 2021.

[5] K. Rajashekara, "Present status and future trends in electric vehicle propulsion technologies," *IEEE J. Emerg. Sel. Topics Power Electron.*, vol. 1, no. 1, pp. 3–10, Mar. 2013.

[6] T. A. Huynh, M.-F. Hsieh, K.-J. Shih, and H.-F. Kuo, "An investigation into the effect of PM arrangements on PMa-SynRM performance," *IEEE Trans. Ind. Appl.*, vol. 54, no. 6, pp. 5856–5868, Nov./Dec. 2017.

[7] S. Panda and R. K. Keshri, "Evaluation of permanent magnet assisted synchronous reluctance motor for light electric vehicle applications," in *Proc. IEEE Int. Conf. Power Electron., Smart Grid Renew. Energy (PESGRE)*, Jan. 2020, pp. 1–6.

[8] M. Paradkar and J. Boecker, "Design of a high performance ferrite magnet-assisted synchronous reluctance motor for an electric vehicle," in *Proc. 38th Annu. Conf. IEEE Ind. Electron. Soc. (IECON)*, Oct. 2012, pp. 4099–4103.

[9] M. Obata, S. Morimoto, M. Sanada, and Y. Inoue, "Performance of PMASynRM with ferrite magnets for EV/HEV applications considering productivity," *IEEE Trans. Ind. Appl.*, vol. 50, no. 4, pp. 2427–2435, Jul./Aug. 2014.

[10] J.-C. Son, J.-M. Ahn, J. Lim, and D.-K. Lim, "Optimal design of PMa-SynRM for electric vehicles exploiting adaptive-sampling Kriging algorithm," *IEEE Access*, vol. 9, pp. 41174–41183, 2021.

[11] H. Cai, B. Guan, and L. Xu, "Low-cost ferrite PM-assisted synchronous reluctance machine for electric vehicles," *IEEE Trans. Ind. Electron.*, vol. 61, no. 10, pp. 5741–5748, Oct. 2014.

[12] E. Carraro, M. Morandin, and N. Bianchi, "Traction PMASR motor optimization according to a given driving cycle," *IEEE Trans. Ind. Appl.*, vol. 52, no. 1, pp. 209–216, Jan./Feb. 2016.

[13] T. Tokuda, M. Sanada, and S. Morimoto, "Influence of rotor structure on performance of permanent magnet assisted synchronous reluctance motor," in *Proc. Int. Conf. Electr. Mach. Syst.*, Nov. 2009, pp. 1–6.

[14] B. Gaussens, J. Boisson, A. Abdelli, L. Favre, and D. Bettoni, "Torque ripple mitigation of PM-assisted synchronous reluctance machine : Design and optimization," in *Proc. 20th Int. Conf. Electr. Mach. Syst. (ICEMS)*, Aug. 2017, pp. 1–6.

[15] Y. Wang, D. M. Ionel, M. Jiang, and S. J. Stretz, "Establishing the relative merits of synchronous reluctance and PM-assisted technology through systematic design optimization," *IEEE Trans. Ind. Appl.*, vol. 52, no. 4, pp. 2971–2978, Jul./Aug. 2016.

[16] P. Li, W. Ding, and G. Liu, "Sensitivity analysis and design of a high performance permanent-magnet-assisted synchronous reluctance motor for EV application," in *Proc. IEEE Transp. Electrific. Conf. Expo (ITEC)*, Jun. 2018, pp. 406–411.

[17] G. Bacco, N. Bianchi, and H. Mahmoud, "A nonlinear analytical model for the rapid prediction of the torque of synchronous reluctance machines," *IEEE Trans. Energy Convers.*, vol. 33, no. 3, pp. 1539–1546, Sep. 2018.

[18] S. A. Mirnikjoo, K. Abbaszadeh, and S. E. Abdollahi, "Multiobjective design optimization of a double-sided flux switching permanent magnet generator for counter-rotating wind turbine applications," *IEEE Trans. Ind. Electron.*, vol. 68, no. 8, pp. 6640–6649, Aug. 2021.

[19] A. Siadatan and M. Karami, "Optimum design of double sided linear switched reluctance motor with Taguchi method," in *Proc. IEEE 28th Int. Symp. Ind. Electron. (ISIE)*, Jun. 2019, pp. 354–358.

MARYAM NASEH received the B.S. degree in electrical engineering from the University of Qom, Qom, Iran, in 2019, and the M.Sc. degree in electrical engineering from the Qom University of Technology, Qom, in 2021. Her research interests include power electronics and electrical machines.

SAEED HASANZADEH received the B.Sc. degree in electrical engineering from the Shahroud University of Technology, Shahroud, Iran, in 2003, and the M.Sc. and Ph.D. degrees in electrical engineering from the University of Tehran (UT), Tehran, Iran, in 2006 and 2012, respectively. His M.Sc. thesis and Ph.D. dissertation have been conducted in the field of high voltage engineering and wireless power transfer (WPT), respectively. In 2013, he joined the Department of Electrical and Computer Engineering, Qom University of Technology, as an Assistant Professor. He was also recognized as an Outstanding Lecturer with the Qom University of Technology, in 2020. He is currently the Dean of the Department of Electrical and Computer Engineering (ECE), Qom University of Technology. His current research interests include power electronics, electrical machines, wireless power transfer, and high-voltage engineering. He is a TPC Member of the IEEE Power Electronics & Drives: Systems and Technologies Conference (PEDSTC). He was a recipient of the Top Research Prize of the Qom University of Technology in 2019. He is an Editorial Board of the Power Electronics Society of Iran (PELSI).

SEYED MOHAMMAD DEHGHAN received the B.Sc. degree in electrical engineering from Azad Islamic University, Yazd, Iran, in 2003, and the M.Sc. and Ph.D. degrees in power engineering from Tarbiat Modares University, Tehran, Iran, in 2005 and 2010, respectively. Since 2011, he has been an Assistant Professor with the Faculty of Electrical and Computer Engineering, Qom University of Technology, Qom, Iran. His research interests include power converters, motor drives, inverter-based distributed generation, electric vehicles, and flexible ac transmission systems.

HOSSEIN REZAEI received the B.S. degree in electrical engineering from Shahid Beheshti University, Tehran, Iran, in 2011, and the M.Sc. degree in electrical engineering from the University of Tehran, Iran, in 2013. He is currently pursuing the Ph.D. degree in electrical engineering with the Babol Noshirvani University of Technology, Iran. His research interests include hybrid and electrical vehicles, electrical machines, and power electronics.

AMEENA SAAD AL-SUMAITI (Senior Member, IEEE) received the B.Sc. degree in electrical engineering from United Arab Emirates University, Al Ain, United Arab Emirates, in 2008, and the M.A.Sc. and Ph.D. degrees in electrical and computer engineering from the University of Waterloo, Waterloo, ON, Canada, in 2010 and 2015, respectively. She was a Visiting Assistant Professor with the Massachusetts Institute of Technology (MIT), Cambridge, MA, USA, in 2017. She is currently an Associate Professor with the Department of Electrical and Computer Engineering, Khalifa University, Abu Dhabi, United Arab Emirates. Her research interests include intelligent systems, energy economics, and energy policy.